Electronic Supplementary Material (ESI) for Journal of Materials Chemistry A.

A conductive selenized polyacrylonitrile cathode in nucleophilic Mg^{2+}/Li^{+} hybrid electrolytes for magnesium/selenium batteries

Hancheng Yuan, Yuanying Yang, Yanna NuLi,* Jun Yang and Jiulin Wang

Supporting Information

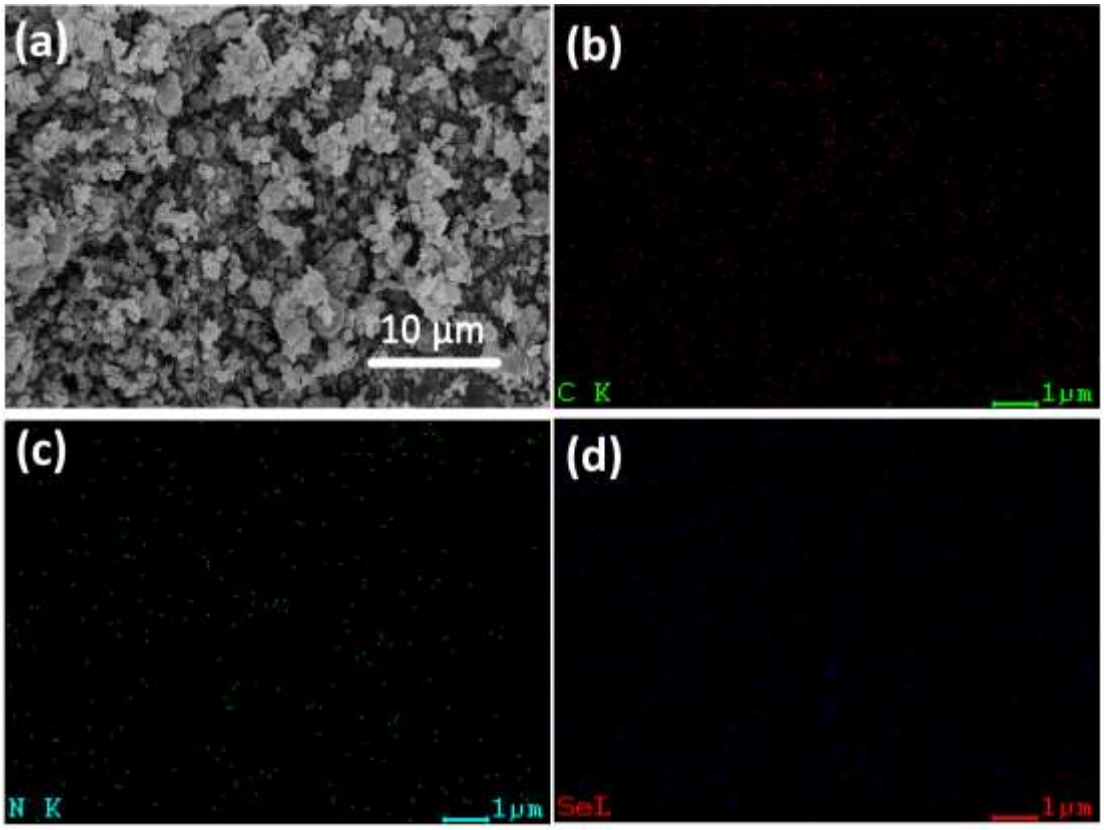

Figure S1. SEM image (a) and the corresponding C (b), N (c) and Se (d) elemental mappings of the Se/PAN composite prepared at 450 ^{o}C for 10h with 8:1 weight ratio of Se and PAN.

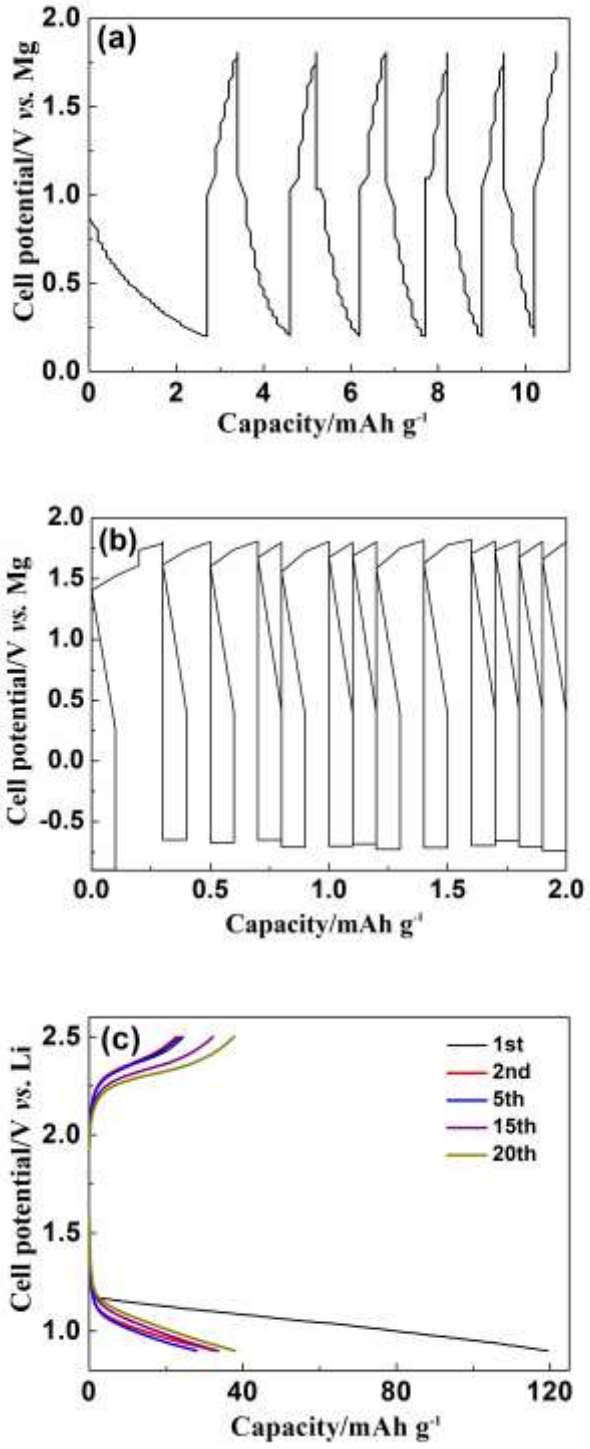

Figure S2. The discharge-charge curves at a rate of 50 mA g^{-1} for Mg-Se/PAN cell with 0.4 mol L^{-1} $(PhMgCl)_2$-$AlCl_3$/THF electrolyte (a), Mg-Se/PAN cell with 1.0 mol L^{-1} LiCl/THF electrolyte (b), and Li-Se/PAN cell with 1.0 mol L^{-1} LiCl/THF electrolyte (c), Se/PAN composite was prepared at 450 ^{o}C for 10h with 8:1 weight ratio of Se and PAN.

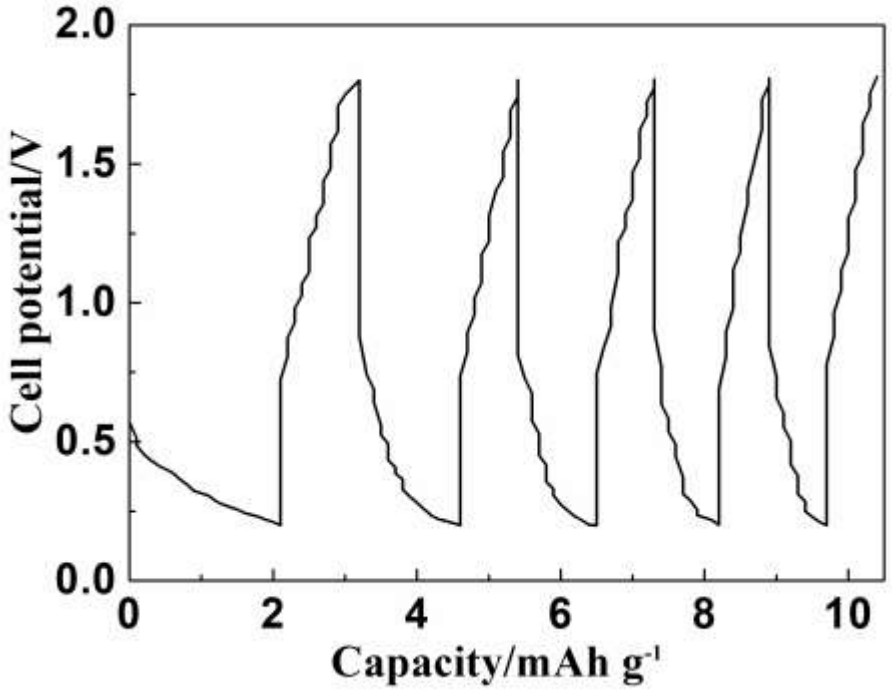

Figure S3. The discharge-charge curves of pyrolyzed PAN heated at 450 ^{o}C at a rate of 50 mA g^{-1} in the electrolyte of 0.4 mol L^{-1} $(PhMgCl)_2$-$AlCl_3$+1.0 mol L^{-1} LiCl /THF.

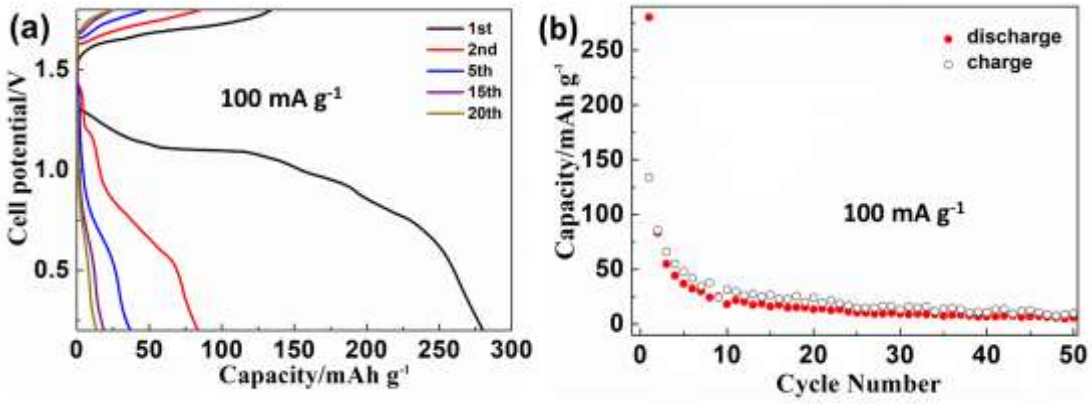

Figure S4. The discharge-charge curves (a) and corresponding cycling performance (b) at a rate of 100 mA g^{-1} for pure Se in the electrolyte of 0.4 mol L^{-1} $(PhMgCl)_2$-$AlCl_3$+1.0 mol L^{-1} LiCl/THF.

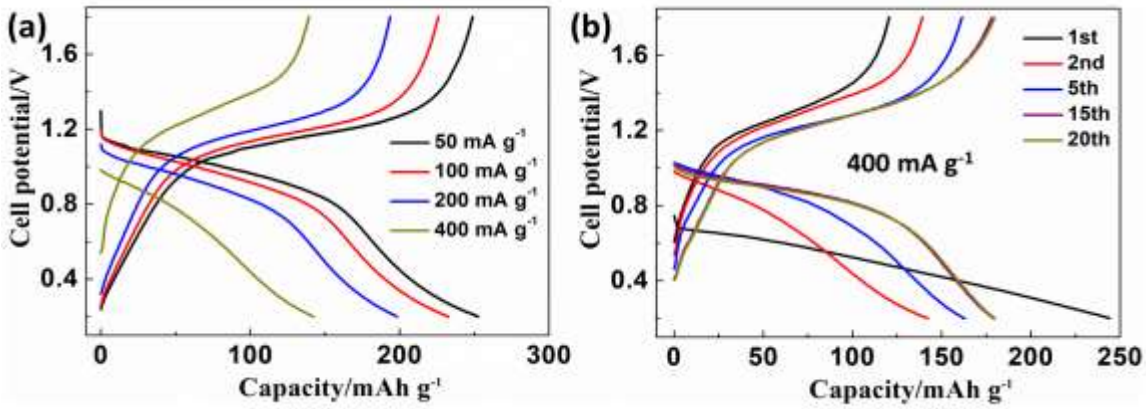

Figure S5. The discharge-charge curves for the second cycle at different current densities (a) and the discharge-charge curves for the 1st, 2nd, 5th, 15th, 20th cycles at a rate of 400 mA g^{-1} (b) of the Se/PAN composite prepared at 450 ^{o}C for 10h with 8:1 weight ratio of Se and PAN in 0.4 mol L^{-1} $(PhMgCl)_2$-$AlCl_3$+1.0 mol L^{-1} LiCl/THF electrolyte.

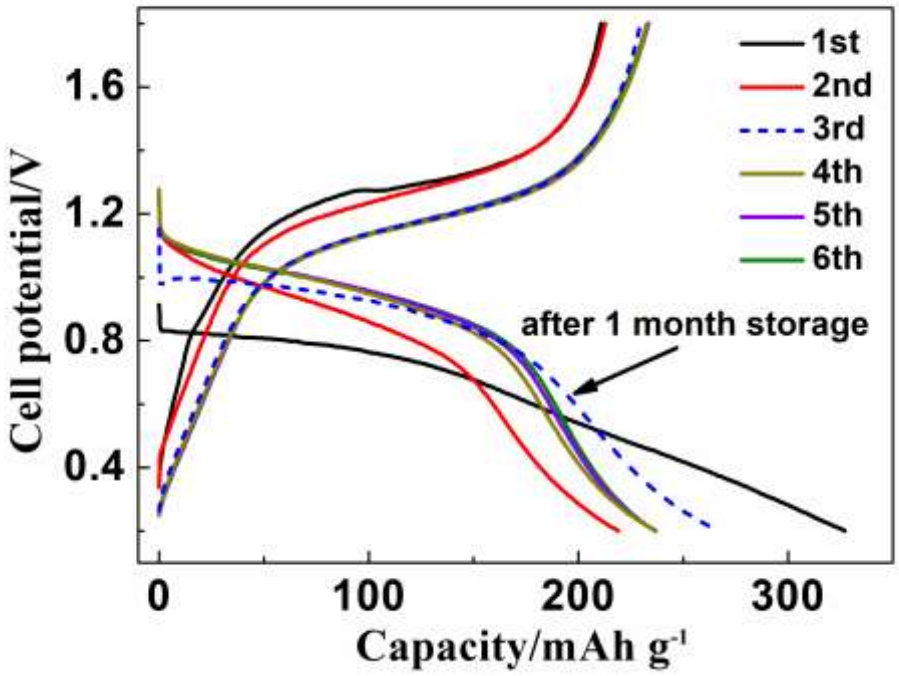

Figure S6. Self-discharge behaviour of the Mg-Se/PAN cell at a rate of 50 mA g^{-1} after 1 month storage in a fully charged state (the 2nd charged state).

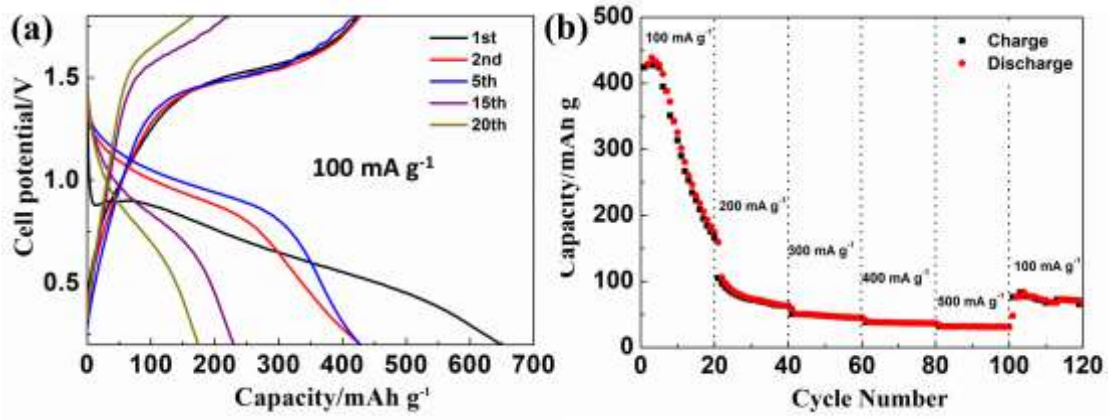

Figure S7. Discharge-charge profiles for S/PAN cathode at a rate of 100 mA g^{-1} (a), and the rate performance at various current densities from 100 mA g^{-1} to 500 mA g^{-1} (b). The electrolyte is 0.4 mol L^{-1} $(PhMgCl)_2$-$AlCl_3$+1.0 mol L^{-1} LiCl/THF.

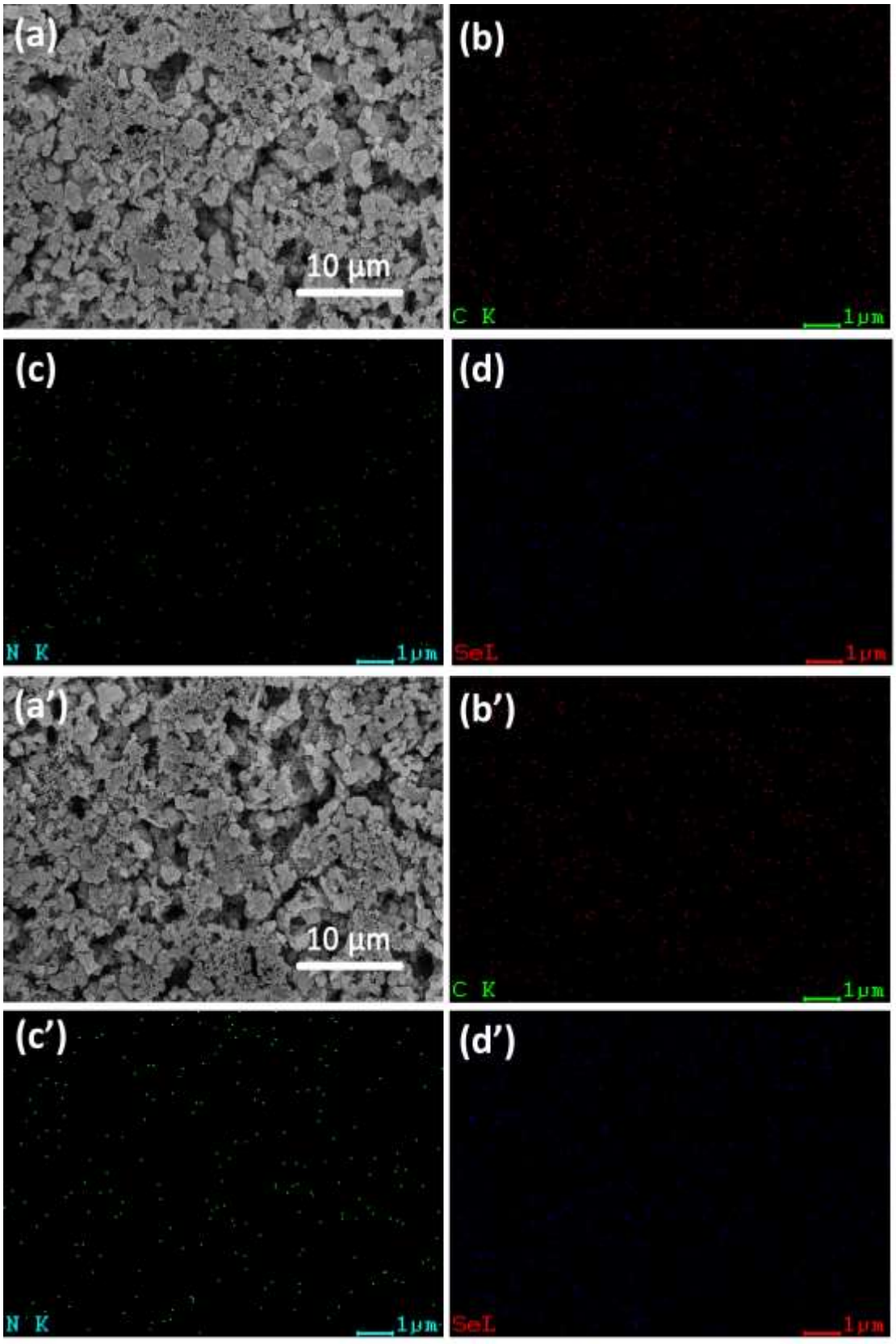

Figure S8. SEM images with corresponding C, N, Se mappings of Se/PAN cathodes before (a, b, c, d) and after 200 cycles (a', b', c', d') at a rate of 100 mA g^{-1}.

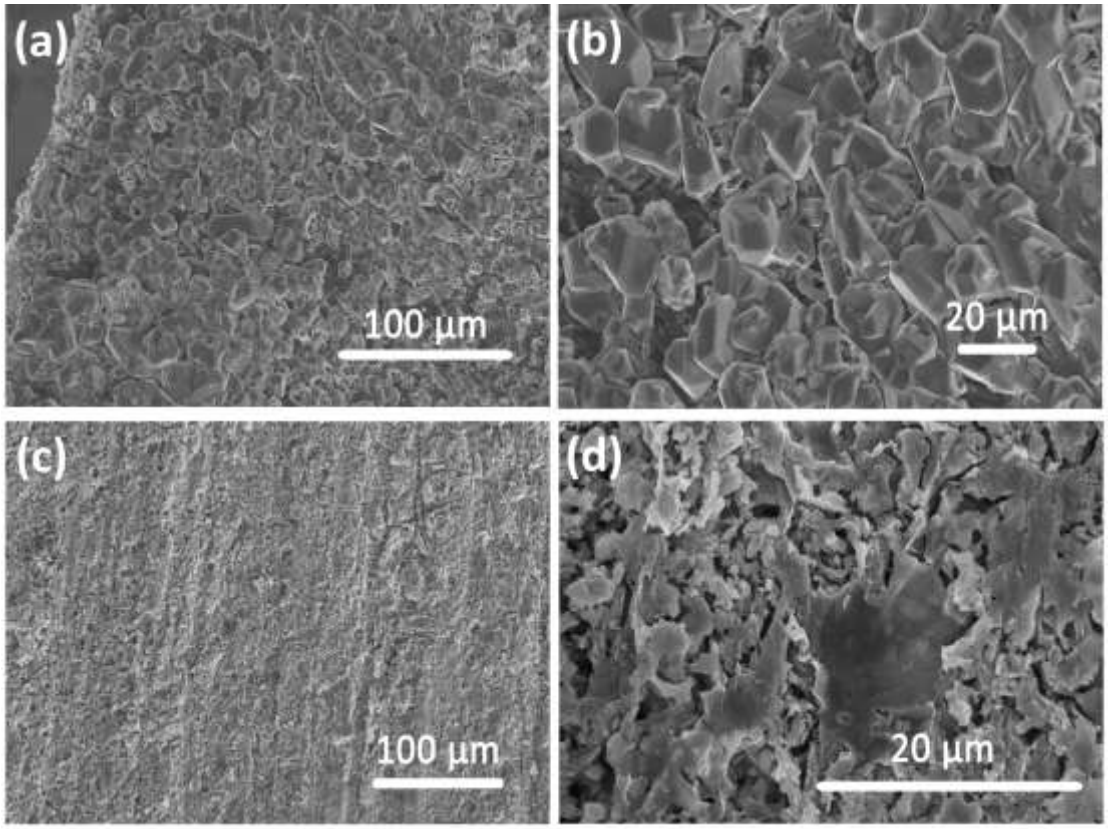

Figure S9. SEM images of Mg anodes after 40 cycles at a rate of 100 mA g^{-1} (a) (b), and after 1000 cycles at a rate of 400 mA g^{-1} (c) (d).

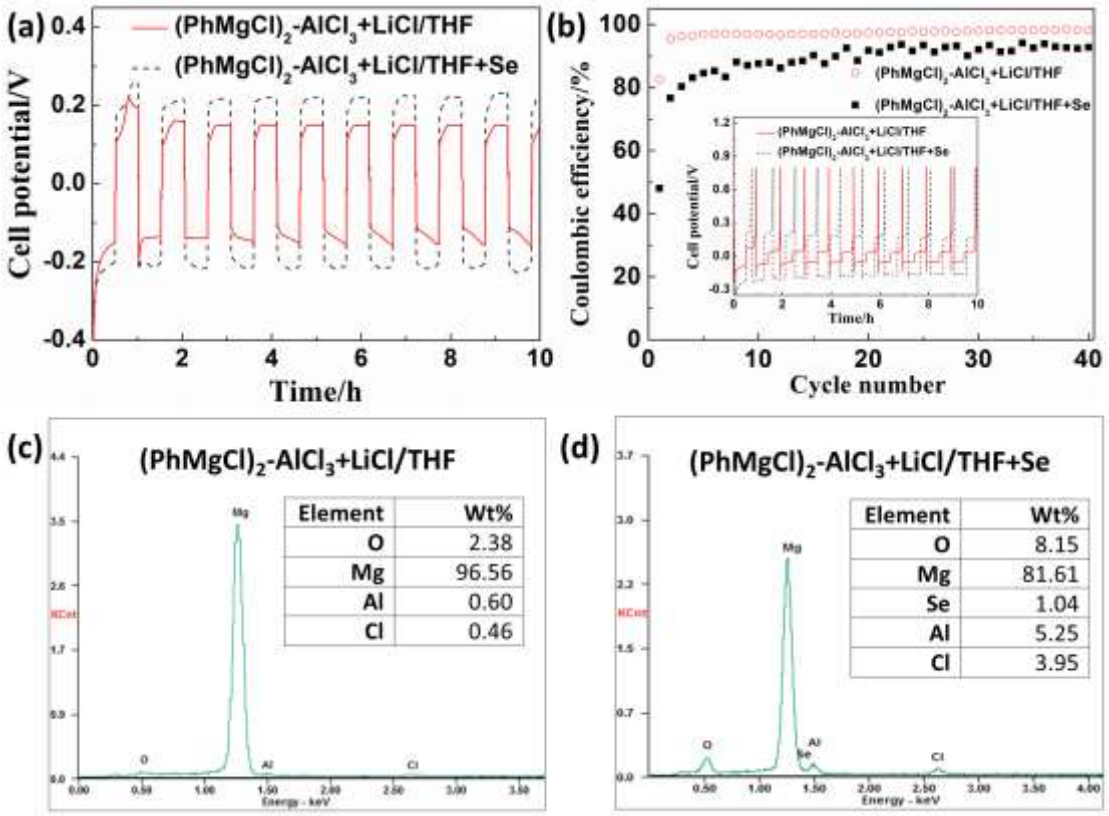

Figure S10. (a) The cycling curves of Mg deposition-dissolution at 0.088 mA cm^{-2} of Mg-Mg cells using the electrolytes of 0.4 mol L^{-1} $(PhMgCl)_2$-$AlCl_3$+1.0 mol L^{-1} LiCl/THF and 0.4 mol L^{-1} $(PhMgCl)_2$-$AlCl_3$+1.0 mol L^{-1} LiCl/THF dissolved with 50 mmol L^{-1} Se. Both discharge and charge are cut off at 30 min. (b) The cycling efficiencies of Mg deposition-dissolution at 0.088 mA cm^{-2} of SS-Mg cells using the electrolytes of 0.4 mol L^{-1} $(PhMgCl)_2$-$AlCl_3$+1.0 mol L^{-1} LiCl/THF and 0.4 mol L^{-1} $(PhMgCl)_2$-$AlCl_3$+1.0 mol L^{-1} LiCl/THF dissolved with 50 mmol L^{-1} Se. Discharge is cut off at 30 min and charge is cut off at 0.8 V, inset is the corresponding cycling curves of Mg deposition-dissolution. EDX spectra of Mg electrodes obtained from cycled cells in 0.4 mol L^{-1} $(PhMgCl)_2$-$AlCl_3$+1.0 mol L^{-1} LiCl/THF electrolyte (c) and 0.4 mol L^{-1} $(PhMgCl)_2$-$AlCl_3$+1.0 mol L^{-1} LiCl/THF dissolved with 50 mmol L^{-1} Se (d).

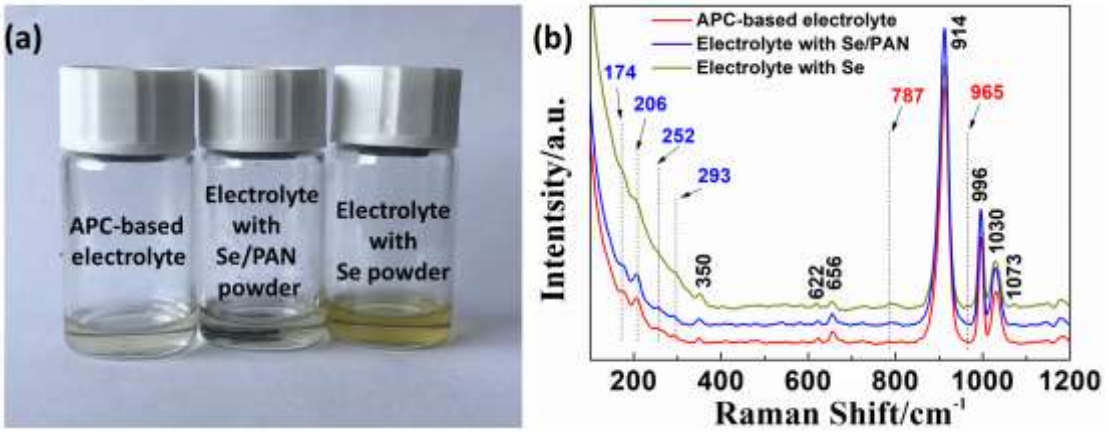

Figure S11. The photo (a) and Raman spectra (b) of 0.4 mol L^{-1} $(PhMgCl)_2$-$AlCl_3$+1.0 mol L^{-1} LiCl/THF electrolyte and the electrolytes after soaking Se/PAN and Se powders for about 48 h, respectively.

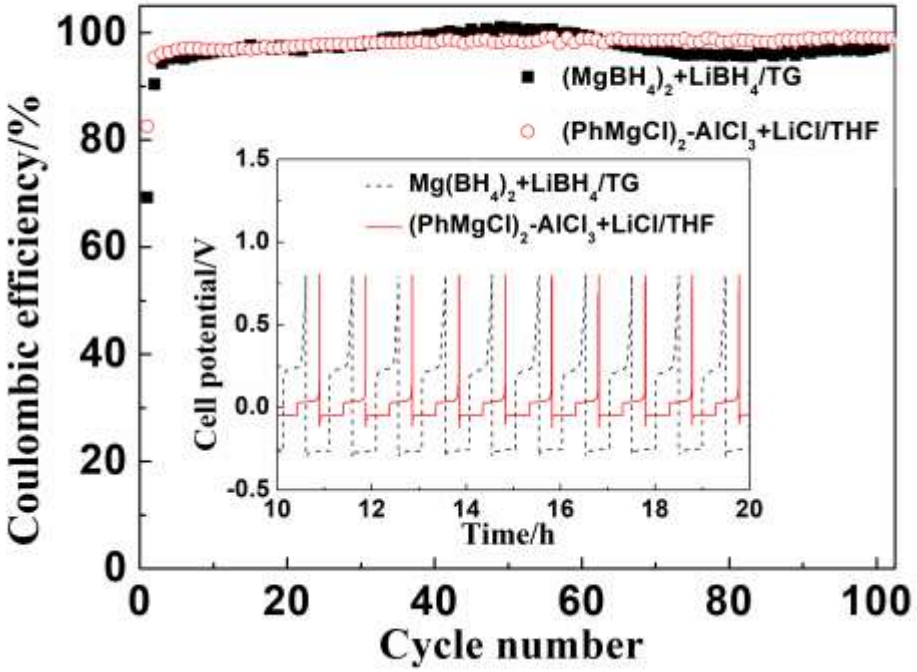

Figure S12. The cycling efficiencies of Mg deposition-dissolution on SS substrate at 0.088 mA cm^{-2} from 0.5 mol L^{-1} $Mg(BH_4)_2$+1.5 mol L^{-1} $LiBH_4$/TG and 0.4 mol L^{-1} $(PhMgCl)_2$-$AlCl_3$+1.0 mol L^{-1} LiCl/THF electrolytes, inset is the cycling curves of Mg deposition-dissolution.

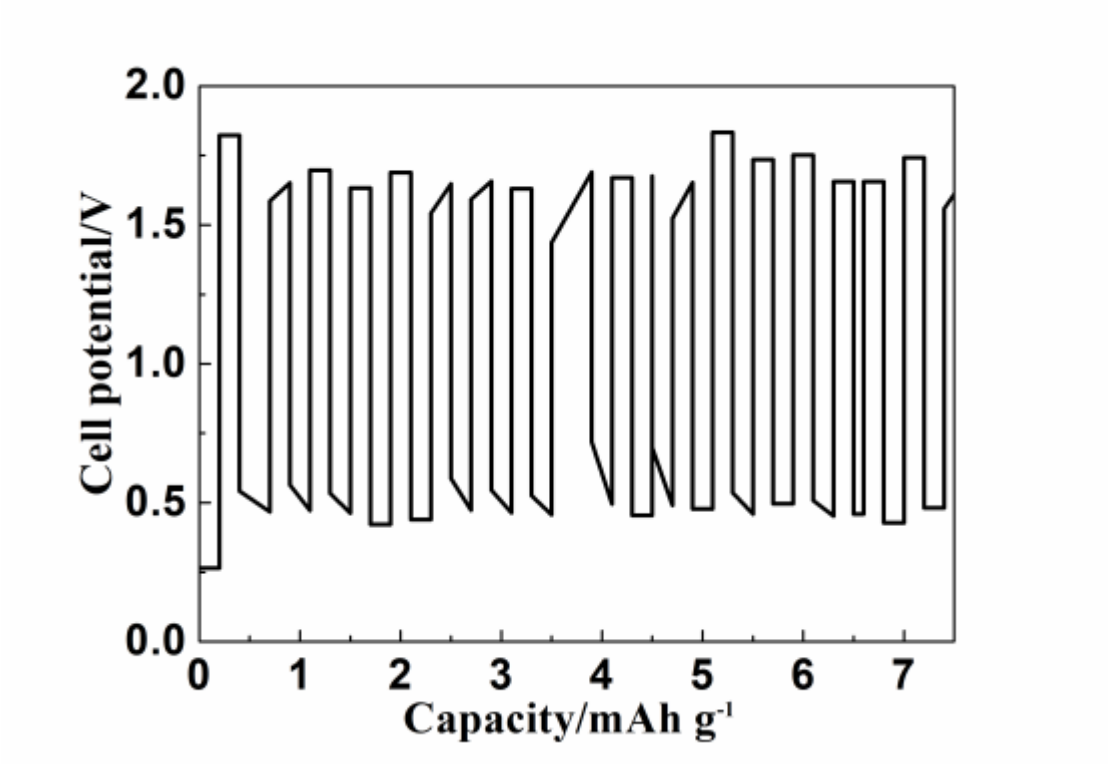

Figure S13. The discharge-charge curves at a rate of 100 mA g^{-1} for pure Se in the electrolyte of 0.5 mol L^{-1} $Mg(BH_4)_2$+1.5 mol L^{-1} $LiBH_4$/TG electrolyte.

Figure S14. The photo of the 0.5 mol L^{-1} $Mg(BH_4)_2$+1.5 mol L^{-1} $LiBH_4$/TG electrolyte, after soaking the Se/PAN electrode and Se electrode for about 5 min.

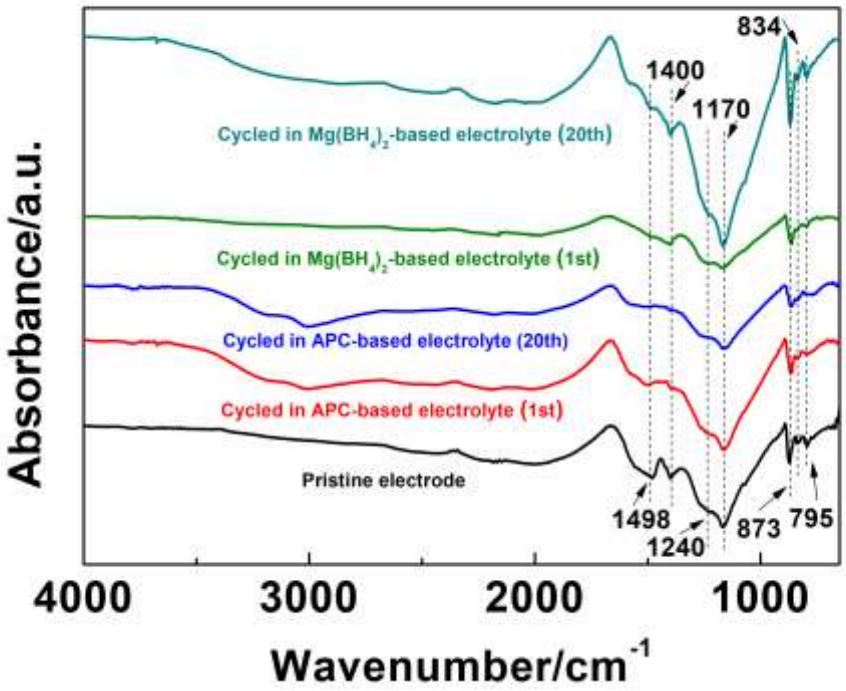

Fig. S15. FITR spectra of pristine Se/PAN electrode and the electrodes cycled in the APC-based electrolyte and the $Mg(BH_4)_2$-based electrolyte at 400 mA g^{-1}.

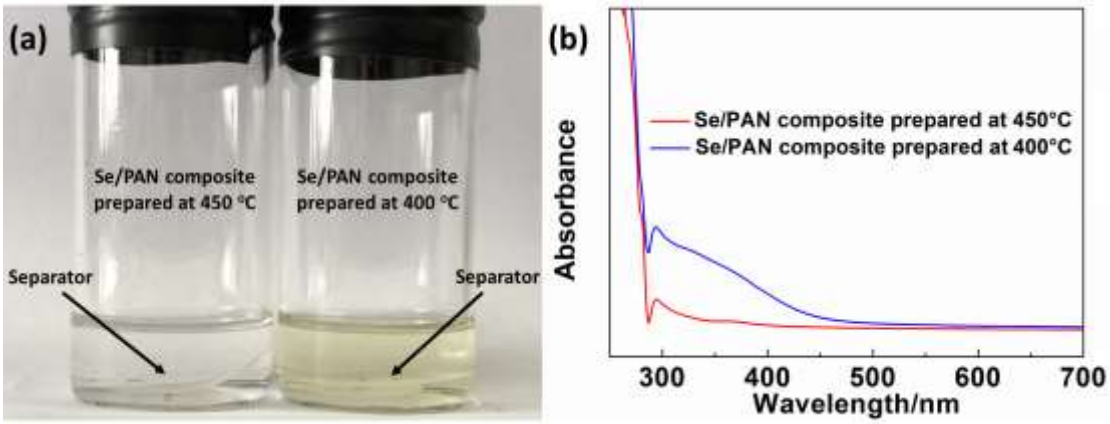

Figure S16. (a) Photo (a) and UV-Vis spectra (b) of THF solutions soaking separators collected from the cycled Mg-Se/PAN cells with 0.4 mol L^{-1} $(PhMgCl)_2$-$AlCl_3$+1 mol L^{-1} LiCl/THF electrolyte after three cycles at 100 mA g^{-1}, Se/PAN composites were prepared at 400 ^{o}C and 450 ^{o}C for 10h with 8:1 weight ratio of Se and PAN, respectively.

Table S1. The fitting values of the resistance shown in Fig. 7.

	Fresh		after 2 cycles		after 20 cycles	
	R_e(ohm)	R_1 (ohm)	R_e(ohm)	R_1(ohm)	R_e(ohm)	R_1 (ohm)
$(PhMgCl)_2$-$AlCl_3$ +LiCl/THF	16.33	33.94	15.65	29.03	17.72	43.96
$(MgBH_4)_2$+$LiBH_4$ /TG	64.57	27.09	61.91	60.82	75.93	193.40

Table S2. Comparison of cycling and rate performance of Mg-Se batteries reported in the literatures with this work.

Cathode material	Se content (wt%)	Electrolyte	Cycling performance		Rate performance		Ref.
			Current density (mA g^{-1}_{Se})	Final discharge capacity (mAh g^{-1}_{Se})/cycle number	Current density (mA g^{-1}_{Se})	Average discharge capacity (mAh g^{-1}_{Se})	
Se/CMK-3	50	0.9 mol L^{-1} $(HMDS)_2Mg$-$(AlCl_3)_2$+0.9 mol L^{-1} $MgCl_2$/TG+DG(1:1)	2 C	100/50	/	/	1
Se/Disordered mesoporous carbon	50	0.5 mol L^{-1} THFPB+0.05 mol L^{-1} MgF_2/DME	66 mA g^{-1} (≈0.1 C)	361/200	1000 mA g^{-1} (≈1.5 C)	405	2
Se/C nanostructures	75	0.5 mol L^{-1} THFPB+0.05 mol L^{-1} MgF_2/DME	0.1 C	607.1/60	/	/	3
Se/PAN composite	45.37	0.4 mol L^{-1} $(PhMgCl)_2$-$AlCl_3$+1 mol L^{-1} LiCl/THF	220 mA g^{-1} (≈0.32 C) 880 mA g^{-1} (≈1.3 C)	415.2/100 260.7/800	1100 mA g^{-1} (≈1.64 C)	355.5	This work

Table S3. FTIR wavenumbers (cm^{-1}) and assignments for Fig. S15.

Wavenumbers (cm^{-1})	Assignments
1498	C=C Stretch[4]
1400	C=C Stretch[5]
1240	C=N Stretch[4]
1170	C-N Stretch
834	C-N Stretch[6]
873	C-Se Stretch[5]
795	Ring Breath (Main-chain Hexahydric-ring)[4]

References:

1 Z. Zhao-Karger, X.-M. Lin, C. B. Minella, D. Wang, T. Diemant, R. J. Behm and M. Fichtner, *J. Power Sources*, 2016, **323**, 213–219.

2 Z. H. Zhang, Z. L. Cui, L.X. Qiao, J. Guan, H. M. Xu, X. G. Wang, P. Hu, H. P. Du, S. Z. Li, X. H. Zhou, S. M. Dong, Z.H. Liu and G. L. Cui, *Adv. Energy Mater.*, 2017, **7**, 1602055.

3 Z. H. Zhang, B. B. Chen, H. M. Xu, Z. L. Cui, S. M. Dong, A. B Du, J. Ma, Q. F. Wang, X. H. Zhou and G. L. Cui, *Adv. Funct. Mater.*, 2018, **28**, 1701718.

4 S. Y. Wei, L. Ma, K. E. Hendrickson, Z. Y. Tu and L. A. Archer, *J. Am. Chem. Soc.*, 2015, **137**, 12143-12152.

5 Z. Iqbal, S. T. Correale, F. Reidinger, R. H. Baughman and Y. Okamoto, *J. Chem. Phy.*, 1988, **88**, 4492-4497.

6 L. C. Zeng, X. Wei, J. Q. Wang, Y. Jiang, W. H. Li and Y. Yu, *J. Power Sources*, 2015, **281**, 461–469.